

---

# Nanoindentation and birefringence measurements on fused silica specimen exposed to low-energy femtosecond pulses

Published September 4, 2006 in Optics Express, Vol. 14, No. 18, p 8360.

In collaboration with:

**Yves Bellouard**

*Micro- & Nano- Scale Eng., Mechanical Eng.  
Dept.,  
Eindhoven University of Technology, PO Box  
513, 5600 MB Eindhoven, The Netherlands*



**Tristan Colomb, Christian Depeursinge**

*Laboratoire d'Optique Appliquée (LOA), Ecole  
Polytechnique Fédérale de Lausanne, STI, IOA,  
Station 17, CH-1015  
Lausanne, Switzerland.*



# Nanoindentation and birefringence measurements on fused silica specimen exposed to low-energy femtosecond pulses

Yves Bellouard

*Micro- & Nano- Scale Eng., Mechanical Eng. Dept.,  
Eindhoven University of Technology, PO Box 513, 5600 MB Eindhoven, The Netherlands.  
[y.bellouard@tue.nl](mailto:y.bellouard@tue.nl)*

Tristan Colomb, Christian Depeursinge

*Laboratoire d'Optique Appliquée (LOA), Ecole Polytechnique Fédérale de Lausanne, STI, IOA, Station 17, CH-1015  
Lausanne, Switzerland.*

Mark Dugan, Ali A. Said, Philippe Bado

*Translume Inc., 6755, Phoenix Drive, Ann Arbor, MI 48108-2222 USA.*

**Abstract:** Femtosecond laser pulses used in a regime below the ablation threshold have two noticeable effects on Fused Silica (a-SiO<sub>2</sub>): they locally increase the material refractive index and modify its HF etching selectivity. The nature of the structural changes induced by femtosecond laser pulses in fused silica is not fully understood. In this paper, we report on nanoindentation and birefringence measurements on fused silica exposed to low-energy femtosecond laser pulses. Our findings further back the hypothesis of localized densification effect even at low energy regime.

©2006 Optical Society of America

**OCIS codes:** (230.1150) All-optical devices; (230.7370) Waveguides; (130.3120) Integrated optics devices; (320.7130) Ultrafast processes in condensed matter, including semiconductors.

---

## References and links

1. X. Liu, D. Du, and G. Mourou, "Laser ablation and micromachining with ultrashort laser pulses," *IEEE J. of Quantum Electron.* **33**, 1706-1716 (1997).
2. K. M. Davis, K. Miura, N. Sugimoto, and K. Hirao, "Writing waveguides in glass with a femtosecond laser," *Opt. Lett.* **21**, 1729-1731 (1996).
3. A. Marcinkevičius, S. Juodkazis, M. Watanabe, M. Miwa, S. Matsuo, H. Misawa, and J. Nishii, "Femtosecond Laser-assisted three-dimensional microfabrication in silica," *Opt. Lett.* **26**, 277-279 (2001).
4. A. Strelsov and N. Borrelli, "Study of femtosecond-laser-written waveguides in glasses," *J. Opt. Soc. Am. B* **19**, 2496-2504 (2002).
5. C. Hnatovsky, R. S. Taylor, E. Simova, P. P. Rajeev, D. M. Rayner, V. R. Bhardwaj, and P. B. Corkum, "Fabrication of microchannels in glass using focused femtosecond laser radiation and selective chemical etching," *Appl. Phys. A* **84**, 47-61 (2006).
6. Y. Bellouard, A. Said, M. Dugan and P. Bado, "Fabrication of high-aspect ratio, micro-fluidic channels and tunnels using femtosecond laser pulses and chemical etching," *Opt. Express* **12**, 2120-2129 (2004).
7. S. Juodkazis, K. Yamasaki, V. Mizeikis, S. Matsuo, and H. Misawa, "Formation of embedded patterns in glasses using femtosecond irradiation," *Appl. Phys. A* **79**, 1549 (2004).
8. S. Juodkazis, H. Misawa, T. Hashimoto, E. G. Gamaly and B. Luther-Davies, "Laser induced microexplosion confined in a bulk of silica: Formation of nanovoids," *Appl. Phys. Lett.* **88**, 201909 (2006).
9. W. C. Oliver and G. M. Phar, "Measurement of hardness and elastic modulus by instrumented indentation: Advances in understanding and refinements to methodology," *J. Mater. Res.* **19**, 3-20 (2004).
10. P. Bado, A. Said, M. Dugan, T. Sosnowski, and S. Wright "Dramatic improvements in waveguide manufacturing with femtosecond lasers," in NFOEC, Dallas, Sept. 2002.
11. T. Colomb, F. Dürr, E. Cuche, P. Marquet, H. Limberger, R.-P. Salathé, and C. Depeursinge, "Polarization microscopy by use of digital holography: application to optical-fiber birefringence measurements," *Appl. Opt.* **44**, 4461-4469 (2005).

12. T. Colomb, E. Cuche, F. Charrière, J. Kühn, N. Aspert, F. Montfort, P. Marquet, and C. Depeursinge, "Automatic procedure for aberration compensation in digital holographic microscopy and applications to specimen shape compensation," *Appl. Opt.* **45**, 851-863 (2006).
13. T. Colomb, F. Montfort, J. Kühn, N. Aspert, E. Cuche, A. Marian, F. Charrière, S. Bourquin, and C. Depeursinge, "Numerical parametric lens for shifting, magnification and complete aberration compensation in digital holographic microscopy," *J. Opt. Soc. Am. A* doc. ID 69126, (posted 5 July 2006, in press).
14. E. Cuche, P. Marquet, and C. Depeursinge, "Spatial filtering for zero-order and twin-image elimination in digital off-axis holography," *Appl. Opt.* **39**, 4070-4075 (2000).

## 1. Introduction

Femtosecond laser pulses interact in unusual ways with matter. In dielectrics, non-linear effects driven by multi-photon absorption are observed [1]. In fused silica ( $\alpha$ -SiO<sub>2</sub>) in particular, various interesting effects of femtosecond laser irradiation have been observed at energy levels below the ablation threshold. Davis *et al.* [2] demonstrated that the refractive index of fused silica can be locally increased and Marcinkevičius *et al.* [3] showed that at higher energy levels (but yet still below the ablation threshold), an increase in etching selectivity to HF acid is observed. Successful applications have been demonstrated since then, but the underlying physical mechanism to explain these two effects remains elusive [4, 5, 6]. Various models have been proposed to explain the observed phenomena, but none has been universally accepted by the scientific community.

The present study aims at improving our knowledge of femtosecond laser irradiation effects on fused silica through novel experimental approaches. More specifically, we used two techniques, nanoindentation and digital holography microscopy to investigate material density changes and related internal stress resulting from the laser exposure.

## 2. Nanoindentation: experimental procedure

We used a Ti:Sapphire femtosecond laser (Coherent RegA) with 100 fs pulses generated at 250 kHz. The focusing optics consists of a 50X objective with a numerical aperture (NA) of 0.55. For these experiments, we used low energy pulses of 25 nJ (check) (as measured after the focusing optics focal lens). This energy regime is particularly interesting for waveguide applications. We use a high purity fused silica substrate (Dynasil® 1100). This glass is characterized by OH content in the range of 600-1000 ppm, a Cl content of 90 ppm and total metallic impurities content 1-2 ppm.

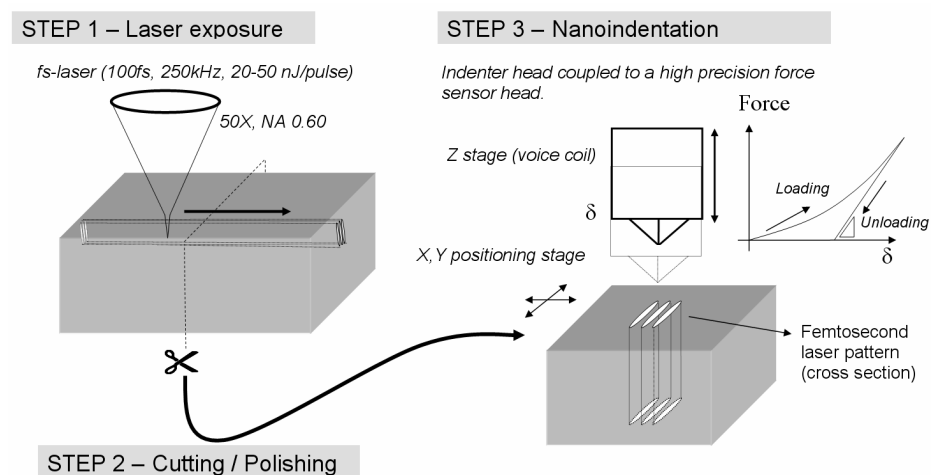


Fig. 1. Schematic of the sample preparation: Step 1, straight lines patterns are written in a piece of fused silica at a depth of 400um; Step 2: the specimen is cut in its middle; Step 3: Nanoindentation experiments. A typical loading/unloading force displacement curve is shown. With CSM technique [9], the stiffness is measured continuously during loading.

The specimen preparation procedure is outlined in Fig. 1. The patterns consist of 5, 7 or 15 parallel lines with a varying pitch of respectively 1.5, 1 and 0.5 microns. The patterns are written 400 microns below the surface. To generate the lines, the laser beam is scanned at a speed of 500 microns/s. Once the patterns are written, the specimen is cut in its middle using a diamond saw. The cut surfaces are polished down to optical transparency. The specimen is visually inspected using a phase contrast optical microscope (Olympus BX 51).

We used a measurement method known as Continuous Stiffness Measurement (CSM) (see Oliver and Pharr [9]). With this technique, the stiffness is measured continuously during the loading of the indenter. This approach provides continuous results as a function of depth and reliable calibration especially when time-dependent plasticity or thermal drift are involved. Furthermore, it facilitates the precise localization of the point of initial contact of the indenter with the sample. We used a Berkovich indenter with a triangular pyramidal shape mounted on the Nanoindenter XP from MTS Systems Corp.

### 3. Nanoindentation: Experimental results

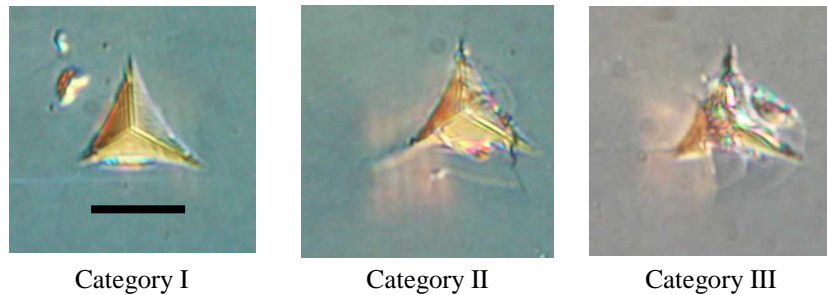


Fig. 2. Example of a nanoindentation mark on laser patterns (scale bar is 10  $\mu\text{m}$ , all three pictures have the same size). The laser patterns are clearly visible under or next to the nanoindenter print.

Nanoindentation is technically rather difficult to implement since the nanoindenter microscope and head are not coaxial resulting in positioning errors. Exact positioning of the tip is nearly impossible. We estimate the positioning accuracy to be about 5  $\mu\text{m}$  for these experiments (this further depends on calibration procedures). Furthermore, nanoindentation is a very sensitive method prone to a variety of experimental errors. To ensure reliable results, it is therefore important to realize a sufficient number of measurements.

We performed a total of 12 nanoindentations on laser irradiated zones of similar structures. After the nanoindentation, the resulting Berkovitch print is inspected in a phase-contrast microscope. We classify our observations in three categories (shown in Fig. 2).

- Category I: the print is rather well aligned with underlying laser pattern and is complete and undeformed. As a criteria, “rather well-aligned” means 50% or more of the print overlaps with the target. (ex. 0 left)
- Category II: the print is misaligned meaning more than 50% of the print body does not overlap with the laser pattern. (ex. 0 middle, note that in this picture some cracks are also identifiable)
- Category III: the print is deformed and cracks are visible. (ex. 0 right)

The results of the nanoindentation test are plotted in Fig. 3. To calibrate the instrument, eight prints were done on the same material but in a region far away from the laser exposed zones. Seven of the eight prints were successful and yielding Young moduli in the range from 71.275 to 72.712 GPa. This value range reflects an average calculated from the large number of data points measured from both the loading and unloading curves using the CSM. The error margin is estimated to be  $\pm 1$  GPa. This calibration was used for all measurements including the bulk reference measurement.

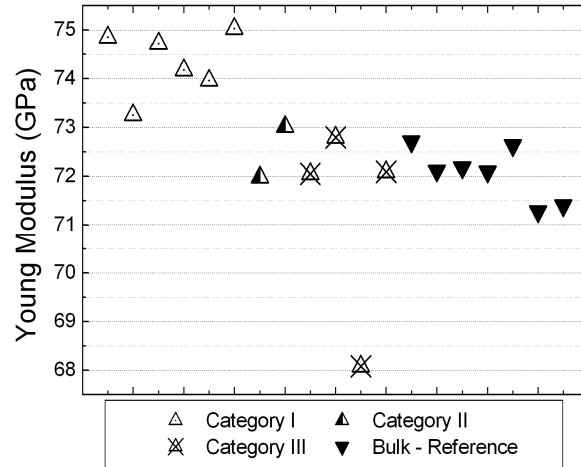


Fig. 3. Overview of nanoindentation tests.

Having in mind all the usual limitations and imprecision inherent to nanoindentation experiments, a consistent trend is observed. For measurement of category I, the Young modulus on the laser pattern, measured in the longitudinal direction is higher in the laser irradiated zone than in the non-irradiated zone. A slight increase of 2 to 3 GPa is observed. The laser pattern has a composite structure being made of parallel lines alternating irradiated and non-irradiated zones. It is therefore difficult to extrapolate from these measurements the effective increase in the laser irradiated zone. Nevertheless, these observations point to structural changes. Combined with other observations reported in Refs. [6, 7, 8, 10], it further supports the hypothesis of localized densification (as suggested in Refs. [6, 7], and recently in Ref. [8]) as a densified region will exhibit an increased Young modulus.

#### 4. Holography-based birefringence measurements: principle.

The holography-based birefringence method is based on the numerical reconstruction of the complete wavefront property (amplitude, phase and polarization state) from a single digital hologram. In particular, a modified digital holographic microscope (DHM) that allows the reconstruction of the wavefront polarization state has been implemented at EPFL [11].

The principle consists of using two reference waves orthogonally polarized that interfere with an object wave. The resulting two wavefronts are reconstructed separately from the same hologram and are processed to image the polarization state in terms of the Jones vector components. A schematic of the actual setup is shown in 0.

The reference waves  $R_1$  and  $R_2$  polarized horizontally (along  $x_{R1}$ ) and vertically (along  $y_{R2}$ ) by polarizers [Pol. in Fig. 4(a)], reach the CCD camera with small incidence angles  $\theta_1$  and  $\theta_2$  respectively. To avoid any interference between the reference waves ( $R_1 \cdot R_2 = R_1 R_2^* = 0$ ), the vectors  $x_{R1}$  and  $y_{R2}$  should be orthogonal; therefore, the directions of propagation  $k_{R1}$  and  $k_{R2}$  should be respectively in the planes  $y_0 z_0$  and  $x_0 z_0$  [0 (b)]. Using the Jones formalism, the different waves are written:

$$\begin{aligned}
 \mathbf{O} &= \begin{pmatrix} |o_1| \exp(i\phi_o) \\ |o_2| \exp i(\phi_o + \Delta\phi_o) \\ 0 \end{pmatrix} = \begin{pmatrix} o_1 \\ o_2 \\ 0 \end{pmatrix} \cdot \exp[i\phi_o], \\
 \mathbf{R}_1 &= \begin{pmatrix} r_1 \\ 0 \\ 0 \end{pmatrix}, \mathbf{R}_2 = \begin{pmatrix} 0 \\ r_2 \\ 0 \end{pmatrix}
 \end{aligned} \tag{1}$$

where  $\phi_o = \phi_o(x,y)$  is the sample optical phase delay seen by a linear horizontal polarized wave and  $\Delta\phi_o$  is the phase difference.

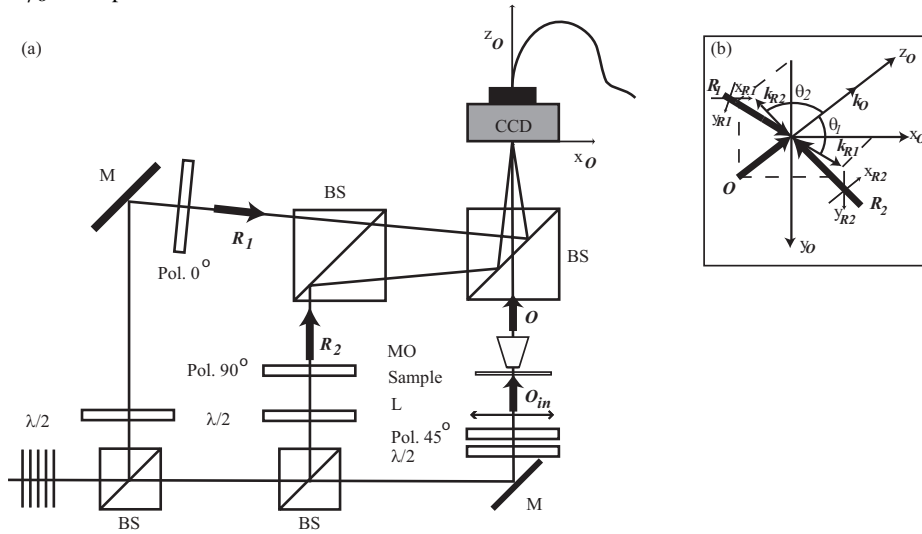


Fig. 4. (a). presents the Pol-DHM set-up designed for transmission imaging with a He-Ne laser source emitting at 633 nm. The basic architecture is that of a Mach-Zehnder interferometer with two orthogonally linearly polarized reference waves  $R_1$  and  $R_2$  that interfere with an object wave  $O$  in off-axis geometry as presented in Fig. 4(b). The state of polarization (SOP) of the object wave  $O$  results from the sample birefringence properties integrated along the propagation direction and of the SOP and depends on the illuminating wave  $O_{in}$ . The linear polarization of  $O_{in}$  is oriented at  $45^\circ$  with a polarizer [Pol.  $45^\circ$  in Fig. 4(a)]. The position of the sample is adjusted to produce a magnified image of the sample with a X63 microscope objective (MO) at a distance  $d$  behind the CCD ( $d \cong 5$  cm).

At the output of the interferometer the interference between  $O$ ,  $R_1$  and  $R_2$  creates the hologram intensity distribution. The hologram contains two fringe patterns corresponding to the interference of the object wave  $O$  with the two reference waves. Because  $R_1$  and  $R_2$  are orthogonal, the two interference fringes correspond to the projection of  $O$  on the base ( $R_1$ ,  $R_2$ ).

The wavefront reconstruction procedure from a digital hologram recorded with a single reference wave is extensively described in Refs. [12, 13]. The procedure consists of illuminating the digital hologram with a digital reference wave having the same propagation direction as the reference wave and propagating the resulting wave to the image plane with the convolution formulation [13].

Here, the same procedure is performed successively with two digital reference waves matching the propagation direction of the two different reference waves. These results in the reconstruction of two numerical complex wavefronts (amplitude and phase) associated with the complex value  $O_1$  and  $O_2$  of Eq. (1). These two wavefronts are then processed as presented in Ref. [11] to image the polarization state in terms of Jones vector components and in particular in term of phase difference  $\Delta\phi_o$ .

An important point is that the DHM technique does not suffer from scattered light in determining the birefringence for two reasons. First, the intensity contributions of the scattered and transmitted lights are very different: the scattered light can be easily neglected. Second, the propagation direction of the scattered light is different from the transmitted light. Therefore, even if the scattered light interferes with the reference waves, the resulting interferences are suppressed by a numerical spatial filtering in the hologram spectrum, as described in Ref. [14]. Only the spatial frequencies associated with the transmitted light remains. Finally, the phase difference  $\Delta\phi_o$  gives an absolute value of the stress as presented in Ref. [11] for a bent optical fiber.

## 5. Holography-based birefringence measurements: results.

For these experiments, single and multiple lines were written in a long slab of fused silica. For the single line (shown on 0), we clearly see a phase difference typically in the order of 2 to 2.5 deg localized along the affected zone. This is rather small effect.

Densely-packed parallel lines (1-micron spacing) were also written using the same processing parameters (0). A typical phase difference of 2 to 2.5 deg was found on the lines. In between lines, the measured phase difference is lower (1 to 1.5 deg).

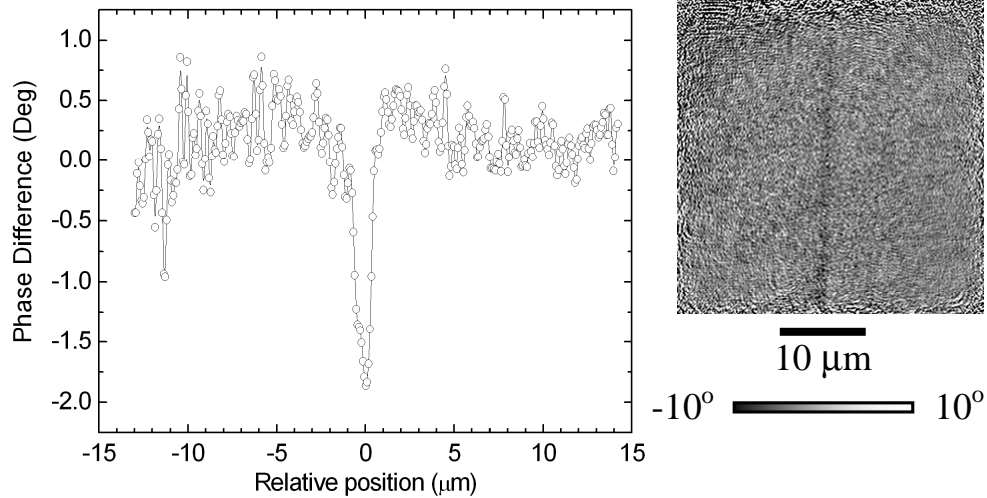


Fig. 5. Measurement of the phase difference along a line perpendicular to a single laser track. The pol-DHM obtained image is shown on the upper right corner.

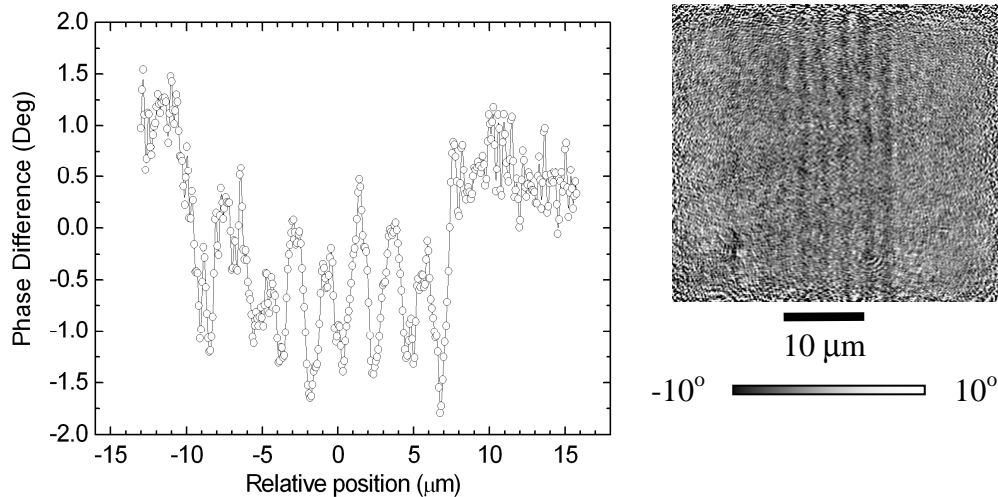


Fig. 6. Phase difference measurement on a set of parallel laser tracks.

## 6. Discussion

Assuming that this birefringence is originating only from the presence of residual stress, one can from these measurements estimate the internal stress. Considering the line geometry, it is assumed that the stress-state is the same for any plane cut perpendicular to the scanned patterns axial direction. Following the model of localized densification, we also make the assumption that the stress is essentially originated from lateral dimension shrinkage.

Using the plane strain approximation, the perturbed refractive indices are given by:

$$\begin{cases} n_x = n_{x0} - C_1 \sigma_x - C_2 (\sigma_y + \sigma_z) \\ n_y = n_{y0} - C_1 \sigma_y - C_2 (\sigma_x + \sigma_z) \end{cases} \quad (2)$$

Where  $n_x, n_y$  represents the perturbed refractive index,  $n_{x0}, n_{y0}$  represents the bulk refractive index,  $\sigma_x, \sigma_y$ , and  $\sigma_z$  are the normal stresses and  $C_1, C_2$  the material photoelastic constants (for fused silica:  $C_1 = 4.2 \cdot 10^{-12} \text{ Pa}^{-1}$ ,  $C_2 = 0.65 \cdot 10^{-12} \text{ Pa}^{-1}$ ). The z-axis is along the laser-pattern direction while the x- and y-axis are in the transverse plane for which the z-axis defined the normal.

In term of phase difference  $\Delta\phi$ , the difference between the two normal stresses of interest can be approximated by,

$$\Delta\sigma = |\sigma_x - \sigma_y| = \frac{\lambda\Delta\phi}{2\pi t(C_2 - C_1)} \quad (3)$$

Where  $\lambda$  is the wavelength of observation (in our case 633 nm), and  $t$  is the thickness of the layer considered. With the focusing optics used, the laser-affected-zone has an ellipsoid-like shape stretched along the femtosecond laser beam direction of propagation. The laser-affected-zone can be estimated using refractive index mapping [10] or through chemical etching and subsequent AFM topography measurement [5]. In our case, the major axis of the laser-affected-zone is estimated to be typically 6 to 10  $\mu\text{m}$ . Using Eq. (3), we find  $\Delta\sigma = 50$  to 80 MPa/deg as an order of magnitude. Therefore the maximum stress difference is estimated to be in the range of 100 to 250 MPa. These are rather high values.

To summarize, laser patterns in fused silica substrates consisting of a set of parallel lines were written with low-energy femtosecond pulses. We used two different experimental methods to investigate local effects of the laser irradiation on fused silica. The nanoindentation experiment indicates that an increased Young modulus is found in the laser-affected-zone. This data is consistent with the model of a localized densification in the region where non-linear absorption has been induced by femtosecond laser exposure.

A different set of specimens consisting of straight lines was made to explore the presence of residual stress through birefringence measurements using Digital Holographic Microscopy (DHM) techniques. Our findings show that DHM measurable stress-induced birefringence spans across 1 to 2 microns. This is slightly larger than the spot size and suggests the presence of residual stress on both sides of each individual laser patterns. However, the stress seems to relax over short distances. This stress is estimated to be in the range of hundred to several hundreds of MPa.

### Acknowledgment

The authors are thankful of the Swiss National Science Foundation for supporting part of this work (research grant 205320-103885/1) and to Christophe Pelletier and Marc van Maris, both from Eindhoven University of Technology, for helping with the nanoindentation experiments.